chapter

20

Digital Image Processing in Nuclear Medicine

Image processing refers to a variety of techniques that are used to maximize the information yield from a picture. In nuclear medicine, computer-based image-processing techniques are especially flexible and powerful. In addition to performing basic image manipulations for edge sharpening, contrast enhancement, and so forth, computer-based techniques have a variety of other uses that are essential for modern nuclear medicine. Examples are the processing of raw data for tomographic image reconstruction in single photon emission computed tomography (SPECT) and positron emission tomography (PET) (see Chapters 16 to 18), and correcting for imaging system artifacts (e.g., Chapter 14, Section B, and Chapter 18, Section D). Another important example is time analysis of sequentially acquired images, such as is done for extracting kinetic data for tracer kinetic models (see Chapter 21). Computer-based image displays also allow three-dimensional (3-D) images acquired in SPECT and PET to be viewed from different angles and permit one to fuse nuclear medicine images with images acquired with other modalities, such as computed tomography (CT) and magnetic resonance imaging (MRI) (see Chapter 19). Computer-based acquisition and processing also permit the raw data and processed image data to be stored digitally (e.g., on computer disks) for later analysis and display.

All of these tasks are performed on silicon-based processor chips, generically called *microprocessors*. The *central processing unit* (CPU) of a general purpose computer, such as a personal computer, is called a *general purpose microprocessor*. Such devices can be programmed to perform a wide variety of tasks, but they are relatively large and not very energy efficient. For very specific tasks, an *application-specific integrated circuit* often is used. ASICs are compact and energy efficient, but their functionality is hardwired into their design and cannot be changed. Examples of their uses include digitizing signals (analog-to-digital converters) and comparing signal amplitudes (pulse-height analyzers and multichannel analyzers). Other categories of microprocessors include *digital signal processors* (DSPs) and *graphics processing units*. These devices have limited programmability, but they are capable of very fast real-time signal and image processing, such as 3-D image rotation and similar types of image manipulations.

The technology of microprocessors and computers is undergoing continuous and rapid evolution and improvement, such that a "state-of-the-art" description rarely is valid for more than a year or, in some cases, even a few months. However, the end result is that the usage of computers and microprocessors in nuclear medicine is ubiquitous. They are used not only for acquisition, reconstruction, processing, and display of image data but also for administrative applications such as scheduling, report generation, and monitoring of quality control protocols.

In this chapter, we describe general concepts of digital image processing for nuclear medicine imaging. Additional discussions of specific applications are found in Chapters 13 to 19 and Chapter 21.

A. DIGITAL IMAGES

1. Basic Characteristics and Terminology

For many years, nuclear medicine images were produced directly on film, by exposing the film to a light source that produced flashes of light when radiations were detected by the imaging instrument. As with ordinary photographs, the image was recorded with a virtually continuous range of brightness levels and x-y locations on the film. Such images sometimes are referred to as *analog images*. Very little could be done in the way of "image processing" after the image was recorded.

Virtually all modern nuclear medicine images are recorded as *digital images*. This is required for computerized image processing. A digital image is one in which events are localized (or "binned") within a grid comprising a finite number of discrete (usually square) picture elements, or *pixels* (Fig. 20-1). Each pixel has a digital (nonfractional) location or *address,* for example, "$x = 5$, $y = 6$." For a gamma camera image, the area of the detector is divided into the desired number of pixels (Fig. 20-2). For example, a camera with a field-of-view of 40 cm × 40 cm might be divided into a 128 × 128 grid of pixels, with each pixel therefore measuring 0.3125 mm × 0.3125 mm. Each pixel corresponds to a range of possible physical locations within the image. If an event were determined to have interacted at a location $x = 4.8$ cm, $y = 12.4$ cm, the appropriate pixel location for this event would be

$$\text{x-pixel location} = 4.8\ \text{cm}/0.3125\ \text{cm/pixel} = \text{int}(15.36) = 15$$

$$\text{y-pixel location} = 12.4\ \text{cm}/0.3125\ \text{cm/pixel} = \text{int}(39.68) = 40$$

where int(x) denotes the nearest integer of x, and the pixels are labeled from 0-127 with the coordinate system defined as shown in Figure 20-2.

A similar format is used for digital multislice tomographic images, except that the discrete elements of the image would correspond to discrete 3-D volumes of tissue within a cross-sectional image. The volume is given by the product of the x- and y-pixel dimensions multiplied by the slice thickness. Thus they are more appropriately called volume elements, or *voxels*. However, when discussing an individual tomographic slice, the term *pixel* still is commonly used. In tomographic images, the "intensity" of each voxel may or may not have a discrete integer value. For example, voxel values for a reconstructed image will generally have noninteger values corresponding to the calculated concentration of radionuclide within the voxel.

Depending on the mode of acquisition (discussed in Section A.4), either the x-y address of the pixel in which each event occurs, or the pixel value, $p(x,y)$, is stored in computer memory. For 3-D imaging modes, such as 3-D SPECT or PET, individual events are localized within a 3-D matrix of voxels, and the reconstructed value in a voxel is denoted as $v(x,y,z)$. Depending on how data are acquired and processed by the imaging system, the pixel or voxel value may correspond to the number of counts, counts per unit time, the reconstructed pixel or voxel value, or absolute radionuclide concentrations (kBq/cc or μCi/cc).

Although most interactions between the user and a computer system involve conventional decimal numbers, the internal operations of the computer usually are performed using *binary numbers*. Binary number representation uses powers of 2, whereas the commonly used decimal number system uses powers of 10. For example, in decimal representation, the number 13 means $[(1 \times 10^1) + (3 \times 10^0)]$. In the binary number system, the same number is represented as 1101, meaning $[(1 \times 2^3) + (1 \times 2^2) + (0 \times 2^1) + (1 \times 2^0)]$, or $(8 + 4 + 0 + 1) = 13$. Each digit in the binary number representation is called a *bit* (an abbreviation

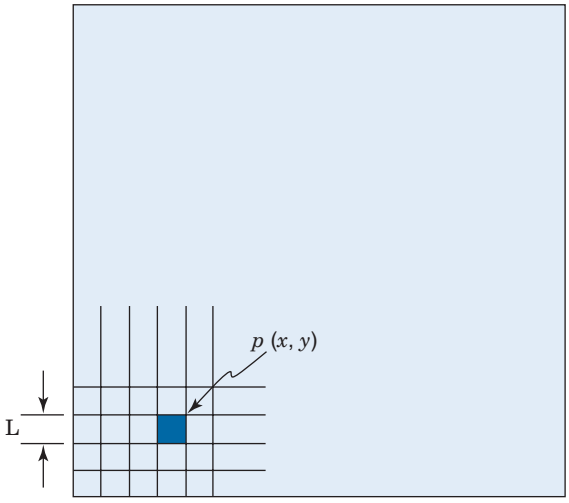

FIGURE 20-1 A digital image consists of a grid or matrix of pixels, each of size L × L units. Each pixel has an x-y address location, with pixel value, $p(x,y)$, corresponding to the number of counts or other quantity associated with that pixel.

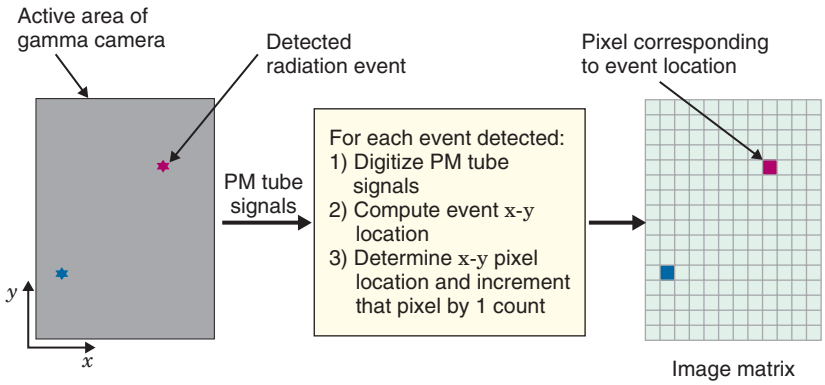

FIGURE 20-2 Subdivision of the gamma camera detector area for generating a digital image. The photomultiplier tube signals are analyzed using analog-to-digital converters to assign the digital matrix location for each detected event.

for "*bi*nary digi*t*"). In general, an n-bit binary number can represent decimal numbers with values between zero and $(2^n - 1)$.

Binary numbers are employed in computer systems because they can be represented conveniently by electronic components that can exist only in an "on" or "off" state. Thus an n-bit binary number can be represented by the "on" or "off" state of a sequence of n such components. To communicate sensibly with the outside world, the binary numbers used within the computer must be converted into decimal integers or into decimal numbers and fractions. The latter are called *floating point* numbers. The methods by which binary numbers are converted to decimal format are beyond the scope of this presentation and can be found in more advanced texts on computer systems.

Digital images are characterized by matrix size and pixel depth. *Matrix size* refers to the number of discrete picture elements in the matrix. This in turn affects the degree of spatial detail that can be presented, with larger matrices generally providing more detail. Matrix sizes used for nuclear medicine images typically range from (64 × 64) to (512 × 512) pixels. Matrix size virtually always involves a power of 2 (2^6 and 2^9 in the previous examples) because of the underlying binary number system used in the computer.

Pixel depth refers to the maximum number of events that can be recorded per pixel. Most systems have pixel depths ranging from 8 bits ($2^8 = 256$; counts range from 0 to 255) to 16 bits ($2^{16} = 65{,}536$; counts range from 0 to 65,535). Note again that these values are related to the underlying binary number system used in the computer. When the number of events recorded in a pixel exceeds the allowed pixel depth, the count for that pixel is reset to 0 and starts over, which can lead to erroneous results and image artifacts.

Pixel depth also affects the number of gray shades (or color levels) that can be represented within the displayed image. In most computer systems in use in nuclear medicine, 8 bits equals a byte of memory and 16 bits equals a word of memory. The pixel depth, therefore, frequently is described as "byte" mode or "word" mode.*

2. Spatial Resolution and Matrix Size

The spatial resolution of a digital image is governed by two factors: (1) the resolution of the imaging device itself (such as detector or collimator resolution) and (2) the size of the pixels used to represent the digitized image. For a fixed field-of-view, the larger the number of pixels, that is, the larger the matrix size, the smaller the pixel size (Fig. 20-3). Clearly, a smaller pixel size can display more image detail, but beyond a certain point there is no further improvement because of resolution limitations of the imaging device itself. A question of practical importance is, At what point does this occur? That is, how many pixels are needed to ensure that significant detail is not lost in the digitization process?

The situation is entirely analogous to that presented in Chapter 16 for sampling requirements in reconstruction tomography. In particular, Equation 16-13 applies—that is, the

*Most modern computer CPUs have 32-bit or 64-bit processors. This means they can process data 32 or 64 bits at a time; however, this is largely independent of image display and how pixel values are stored.

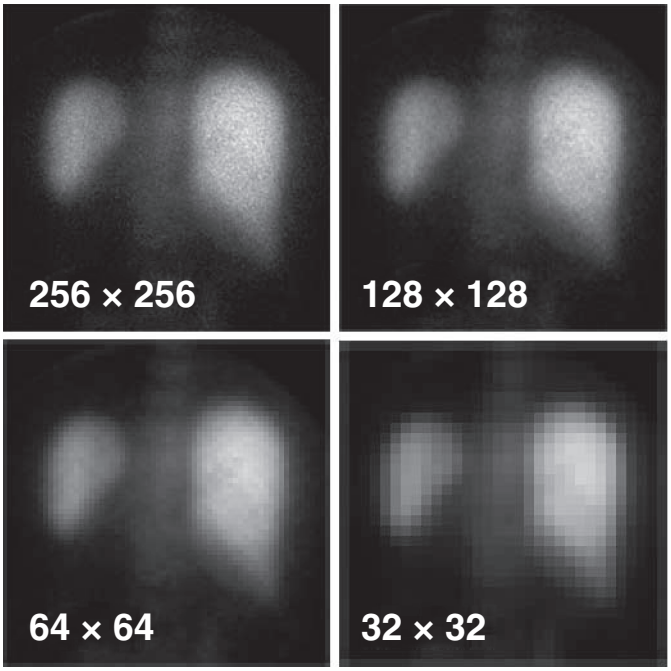

FIGURE 20-3 Digital images of the liver and spleen (posterior view) displayed with different matrix sizes. The larger the matrix size, the smaller the pixels and the more detail that is visible in the image. (*Original image courtesy GE Medical Systems, Milwaukee, WI.*)

linear sampling distance, d, or pixel size, must be smaller than or equal to the inverse of twice the maximum spatial frequency, k_{max}, that is present in the image:

$$d = 1/(2 \times k_{max}) \qquad (20\text{-}1)$$

This requirement derives directly from the sampling theorem discussed in Appendix F, Section C.

Once this sampling requirement is met, increasing the matrix size does not improve spatial resolution, although it may produce a cosmetically more appealing image with less evident grid structure. If the sampling requirements are not met (too coarse a grid), spatial resolution is lost. The maximum spatial frequency that is present in an image depends primarily on the spatial resolution of the imaging device. If the resolution of the device is specified in terms of the full width at half maximum (FWHM) of its line-spread function (Chapter 15, Section B.2), then *the sampling distance (pixel size) should not exceed about one third of this value to avoid significant loss of spatial resolution*, that is,

$$d \lesssim \frac{\text{FWHM}}{3} \qquad (20\text{-}2)$$

This applies for noise-free image data. With added noise it may be preferable to relax the sampling requirement somewhat (i.e., use larger pixels) to diminish the visibility of noise in the final digitized image.

EXAMPLE 20-1

What is the approximate spatial resolution that can be supported for a 30-cm diameter field-of-view using a 64 × 64 matrix? A 128 × 128 matrix? Assume that the original data are noise free.

Answer

64 × 64 matrix

A 64 × 64 image matrix results in a pixel size of 300 mm/64 = 4.69 mm. From Equation 20-2, this would be suitable for image resolution given by

$$\text{FWHM} \gtrsim 3 \times \text{pixel size} = 14.06 \text{ mm}$$

128 × 128 matrix

$$\text{FWHM} \gtrsim 3 \times 300 \text{ mm}/128 = 7.03 \text{ mm}$$

The values calculated in Example 20-1 represent the approximate levels of imaging system resolution that could be supported without loss of imaging resolution for the specified image and matrix sizes. The practical effects of undersampling depend as well on the information contained in the image and whether it has a significant amount of actual spatial frequency content near the

resolution limit of the imaging device. Practical experimentation sometimes is required to determine this for a particular type of imaging procedure.

3. Image Display

Digital images in nuclear medicine are displayed on cathode ray tubes (CRTs) or flat-panel displays such as liquid crystal displays (LCDs). In addition to their use at the site of the imaging device, displays are an essential component of picture archival communications systems (PACS) networks, for remote viewing of images (see Section C). The spatial resolution of the display device should exceed that of the underlying images so as not to sacrifice image detail. In general, the display devices used in nuclear medicine computer systems and in radiology-based PACS networks comfortably exceed this requirement. Typical high-resolution CRTs have 1000 or more lines and a typical LCD might have 1536×2048 elements.

Individual pixels in a digital image are displayed with different brightness levels, depending on the pixel value (number of counts or reconstructed activity in the pixel) or voxel value. On *grayscale* displays, the human eye is capable of distinguishing approximately 40 brightness levels when they are presented in isolation and an even larger number when they are presented in a sequence of steps separated by sharp borders. Image displays are characterized by the potential number of brightness levels that they can display. For example, an 8-bit grayscale display can potentially display $2^8 = 256$ different brightness levels. Such a range is more than adequate in comparison with the capabilities of human vision. In practice, the effective brightness scale often is considerably less than the physical limits of the display device because of image noise. For example, if an image has a root mean square noise level of 1%, then there are not more than 100 significant brightness levels in the image, regardless of the capabilities of the display device.

Digital images also can be displayed in color by assigning color hues to represent different pixel values. The human eye can distinguish millions of different colors, and color displays are capable of producing a broader dynamic range (i.e., number of distinguishably different levels) than can be achieved in black-and-white displays. For example, a *true-color* display with 24-bit graphics can generate nearly 16.8 million different colors [$2^{24} = (2^8)^3$, in which the 3 represents the independently generated red, green, and blue color channels].

One commonly used color scale, the *pseudocolor* scale (sometime known as the *rainbow* or *spectrum* color scale), assigns different colors from the visible spectrum, ranging from blue at the low ("cool") end, through green, yellow, and red ("hot"), for progressively increasing pixel values. This is an intrinsically nonlinear scale, because the viewer does not perceive equal significance for successive color steps. A somewhat more natural scale, the so-called *heat* or *hot-body* scale, assigns different shades of similar colors, such as red, yellow, and white, to progressively increasing pixel values, corresponding to the colors of an object heated to progressively higher temperature. In both examples, the colors are blended to produce a gradual change over the full range of the scale. Figure 20-4 shows the same image displayed with different color scales.

The major problem with the use of color scales to represent pixel count levels is that they are somewhat unnatural and also can produce contours, such as apparently sharp changes in pixel values, where none actually exist. A more practical use of color displays is for color coding a second level of information on an image. For example, in combined-modality imaging of PET or SPECT with CT (see Chapter 19), the anatomic (CT) image often is displayed using a standard gray scale, whereas the functional (PET) image is shown using a color scale. Such a display clearly differentiates between the two types of images, whereas a simple overlay of two grayscale images would be confusing.

Hard-copy images can be produced on black-and-white transparency film from a CRT display. Single-emulsion films are used to minimize blurring of the recorded image, especially when images are minified for compact display on a single sheet of film. The CRT display intensity must be calibrated to compensate for the sensitometric properties of the recording film to match the monitor display. Computer printers are now commonly used to record hard-copy images and a range of different technologies and media are available depending on requirements such as quality (resolution and gray-scale range), cost and printing speed.

4. Acquisition Modes

Digital images are acquired either in frame mode or in list mode. In *frame-mode* acquisition, individual events are sorted into their

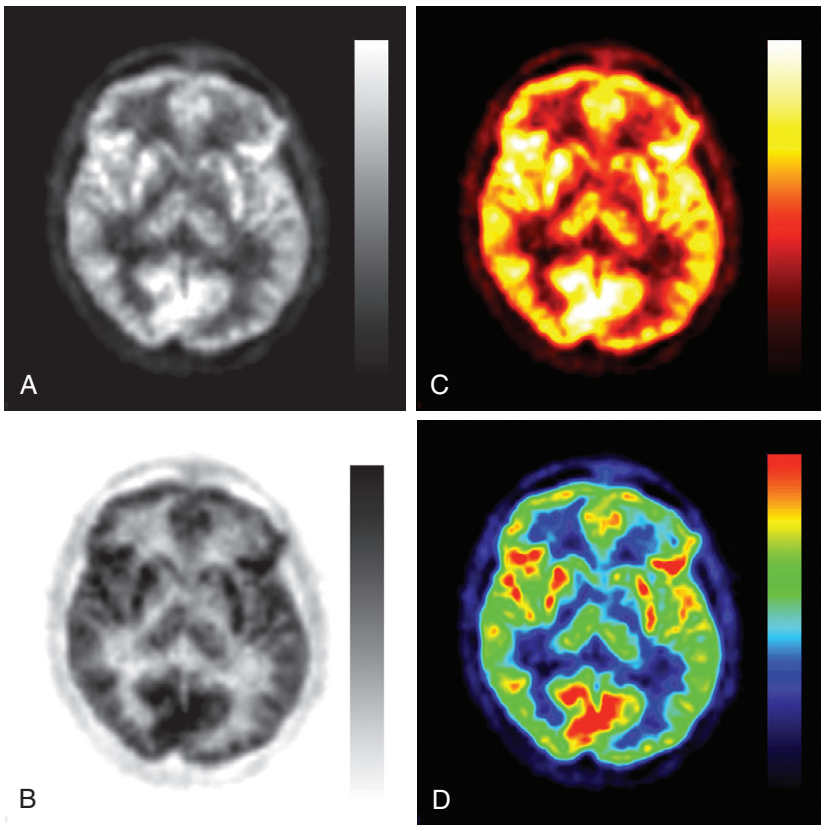

FIGURE 20-4 The same reconstructed transaxial image slice rendered in different color scales. *A,* Grayscale, high-intensity white; *B,* inverted grayscale, high-intensity black; *C,* hot-wire or hot-body scale; *D,* pseudocolor spectral scale. The slice is from a PET scan of the brain using the radiotracer ^{18}F-fluorodeoxyglucose. (*Original image courtesy Siemens Molecular Imaging, Knoxville, TN*).

appropriate x-y locations within the digital image matrix immediately after their position signals are digitized. After a preset amount of time has elapsed or after a preset number of counts have been recorded, the acquisition of data for the image is stopped and the pixel values [$p(x,y)$ = number of counts per pixel] are stored in computer memory.

When a series of such images is obtained sequentially, individual images in the sequence are referred to as "frames." Clearly, the image matrix size (e.g., 64×64, 128×128, and so forth) must be specified before the acquisition begins. Additionally, the time duration of the frame sets a limit on the temporal accuracy of the data. For example, if the frame is acquired during a 1-minute period, the number of counts recorded in each pixel represents the integrated number of counts during the 1-minute acquisition period and cannot be subdivided retrospectively into shorter time intervals. When faster framing rates are used, such as for cardiac blood-pool imaging, temporal sampling accuracy is improved, but the total counts per frame and per pixel are reduced compared with slower frame rates.

In *list-mode* acquisition, the incoming x and y position signals from the camera are digitized, but they are not sorted immediately into an image grid. Instead, the x and y position coordinates for individual events are stored, along with periodic clock markers (e.g., at millisecond intervals). This permits retrospective framing with frame duration chosen after the data are acquired.

List-mode acquisition permits greater flexibility for data analysis. However, it is not an efficient method for using memory space during acquisition for conventional imaging, especially for high-count images, because every recorded event occupies a memory location. Thus a 1-million count 128×128 image recorded in list mode would require 1 million memory locations, whereas in frame mode the same image would require only approximately 16,000 memory locations. However, list mode can actually be more efficient in

some situations. This would apply, for example, if the average number of counts is less than 1 per pixel in an image frame. In this case, list mode would require fewer memory locations to record the image than frame mode. Such situations can arise (e.g., in fast dynamic studies).

Another commonly used acquisition mode is called *gated imaging*. In this mode, data are acquired in synchrony with the heart beat or with the breathing cycle, so that all images are acquired at the same time during the motion cycle. This helps reduce blurring and other possible image artifacts induced by body motion (see Fig. 15-1). To perform gated imaging, it is necessary to have some sort of monitoring system in place, such as electrocardiogram leads for the heart beat or a pneumatically operated "belly band" that produces an electrical signal when it expands during the breathing cycle.

In frame-mode gated imaging, the signals from the motion-monitoring device are used to initiate an image-acquisition cycle. The "cycle" may consist of several images, each of which represents the object at the same location, assuming the motion is repeated reproducibly during the cycle. With list-mode acquisition, retrospective synchronization is possible by recording the motion-monitoring signal along with the signals from the detector. In either case, data usually are acquired over a large number of cycles and the images are added together, until the total number of counts is sufficient to provide adequate counting statistics.

B. DIGITAL IMAGE-PROCESSING TECHNIQUES

All modern nuclear medicine systems are provided with fairly sophisticated software for displaying and processing the images that are acquired on those systems. There also are many "third-party" software packages available that incorporate extensive tools for image processing and allow images from different manufacturers and different modalities to be analyzed. A variety of digital image-processing techniques are used in nuclear medicine, some of which are fully automatic (i.e., performed entirely by the computer), whereas others are interactive (i.e., require some user input). In this section, we describe briefly a subset of the major image-processing tools that are commonly used in nuclear medicine.

1. Image Visualization

Commonly, a single projection image, or in the case of tomographic data, a set of contiguous image slices, are displayed on the screen. The display of the images can be manipulated in a number of ways to aid in interpretation. This includes changing from a linear gray scale to a color scale or to a nonlinear (e.g., logarithmic) gray scale, or limiting the range of pixel values displayed. The latter is known as *windowing*. For example, if greater contrast is desired in one region of an image, the full brightness range of the display device can be used to display only the range of pixel values found within that region (Fig. 20-5). This increases the displayed contrast in the selected area, but other parts of the image may have diminished contrast as a result (i.e., the counts per pixel may be beyond the upper or lower range of the selected grayscale window). Whenever image data are displayed or reproduced, it is desirable to show a gray-scale or color-scale bar that has undergone the same manipulations as the images, so that the viewer can interpret the image in the context of how the display has been modified.

Tomographic nuclear medicine data consists of a 3-D volume that can be displayed in conventional transaxial views or in coronal or sagittal views (Fig. 20-6). Often it is useful to display all three views simultaneously on the screen. Typically, a point within the object is chosen using the cursor, and the three orthogonal images that pass through that point are displayed. As the cursor is moved, the transaxial, coronal, and sagittal images are updated. This is an efficient way of navigating through a large 3-D dataset. The dataset also can be resliced at an arbitrary orientation to provide oblique views. This is useful for objects whose line of symmetry does not fall naturally along one of the perpendicular axes of the 3-D volume. An example is reslicing the 3-D dataset to provide short axis views of the heart.

Another useful visualization tool for 3-D tomographic datasets is the *projection tool*. This collapses the 3-D dataset into a single 2-D image for a specified viewing angle and allows all the data to be seen at once. An example is shown in Figure 20-7. A number of different algorithms are available to "render" the projection images. The simplest approach is to simply sum the intensities along the projection direction. This is essentially equivalent to what would be obtained by acquiring

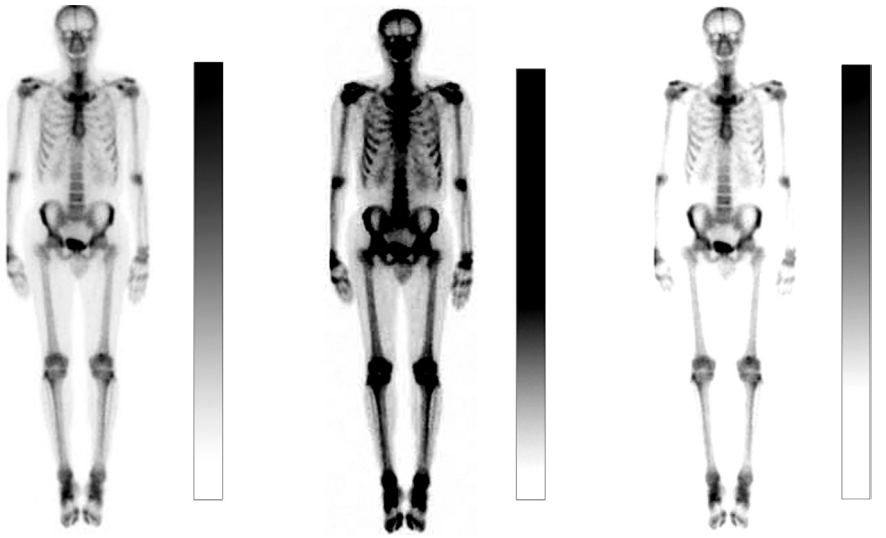

FIGURE 20-5 Effect of changing the distribution of gray levels on image contrast. *Left,* Original image with uniform distribution of gray levels. *Center,* Gray scale compressed (fewer levels) in high-count (*dark*) regions to improve the visualization of soft tissues. *Right,* Gray scale compressed in low-count (*light*) regions to suppress soft tissues and visualize only bone. (*Image courtesy Siemens Medical Solutions, USA, Inc.*)

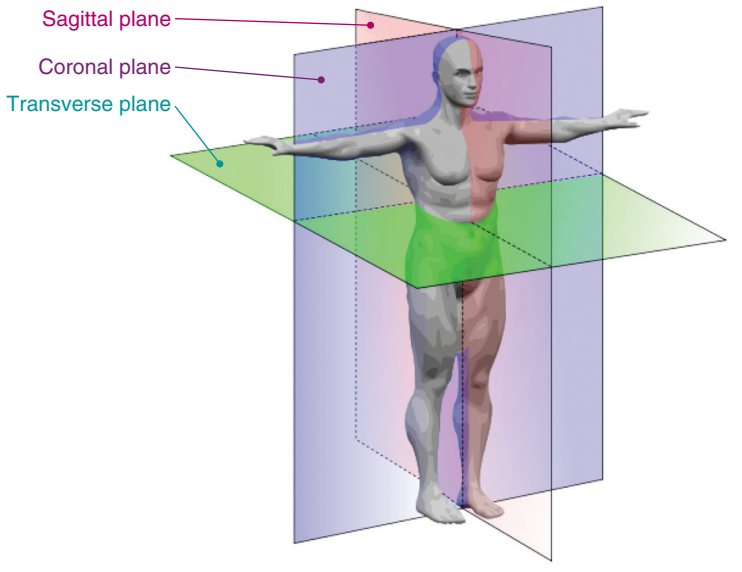

A

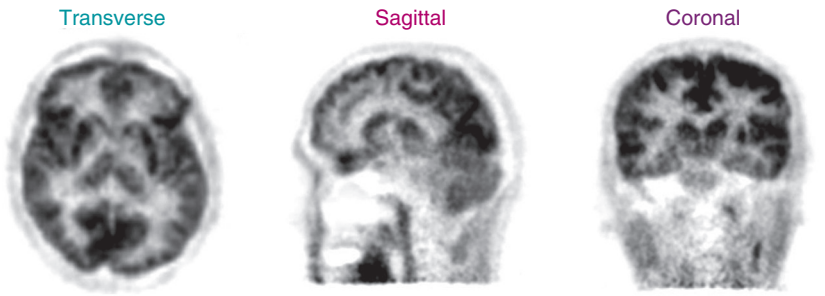

B

FIGURE 20-6 *A,* Orientation of transverse (also known as transaxial), coronal and sagittal sections. *B,* Orthogonal views (transverse, coronal, sagittal) of an ^{18}F-fluorodeoxyglucose PET brain study in which the imaging field-of-view covers the entire head. (*A, Reproduced from* http://en.wikipedia.org/wiki/File:Human_anatomy_planes.svg#file. *B, Images courtesy CTI PET Systems, Inc., Knoxville, TN.*)

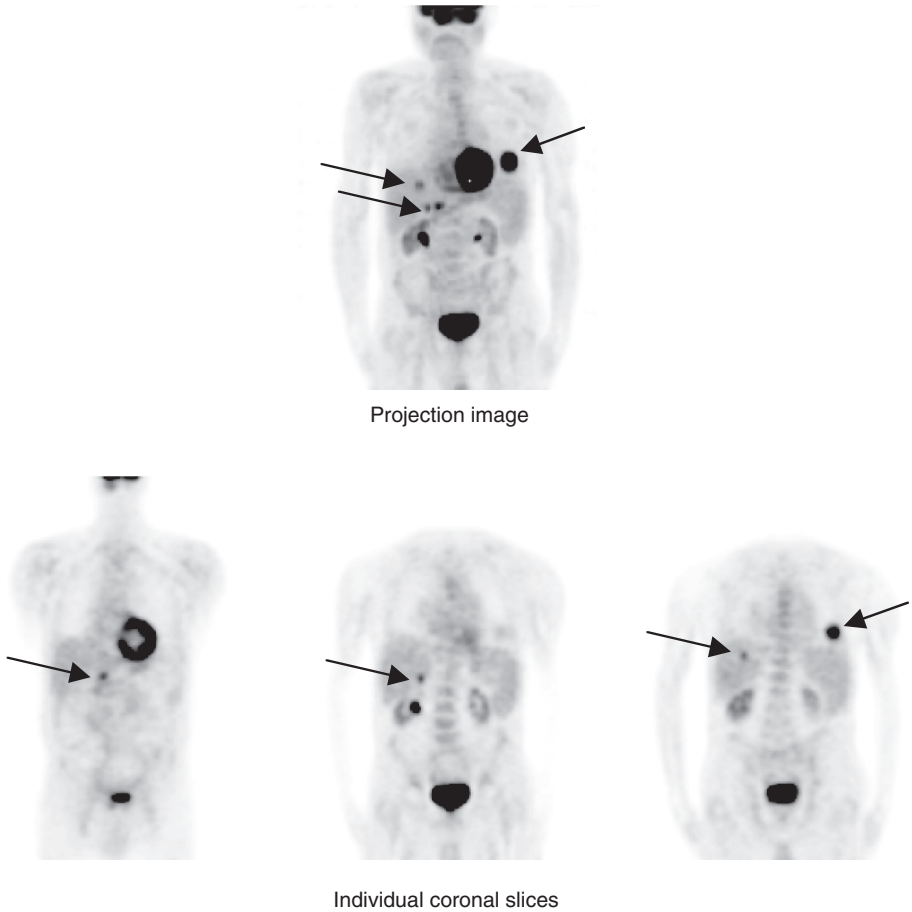

FIGURE 20-7 Whole-body ^{18}F-fluorodeoxyglucose PET study displayed as a single projection image (*top*) and as a series of coronal image slices (*bottom row*). The projection image shows the distribution of radiotracer in all slices (*arrows* correspond to metastatic disease in this patient with cancer), but image resolution and contrast are lost relative to the individual tomographic slices. Projection images often are a convenient way to initially view large tomographic datasets, after which individual tomographic slices can be used for more detailed examination or quantitative analysis. (*Courtesy Dr. Magnus Dahlbom, University of California–Los Angeles.*)

2-D views of the object from many projection directions. Another approach is to display only the surface pixel values (*surface rendering*). An approach that highlights internal features is to display only the pixel with the maximum value along the projection direction (*maximum intensity projection*).

By computing projection views at a set of angles around the object and presenting them in a continuous loop, one can create movies in which it appears that the object is rotating in space. This sometimes is called *cine mode.* These and other rendering and display algorithms are discussed in some of the suggested readings at the end of the chapter.

Another important application of image processing is *image arithmetic.* There are a number of applications in which one wishes to see differences between images or to combine images acquired with different radionuclides or acquired with different modalities. Most image-processing software allows one to add, subtract, multiply, and divide single images or 3-D image volumes. These operations typically are applied on a pixel-by-pixel basis. Figure 20-8 is an example of a simple frame arithmetic operation: subtraction. The study illustrated is a visual stimulation using ^{15}O-labeled water as a flow tracer. Visual stimulation, created by having the subject view a strobe light, caused an increase in blood flow to the occipital (visual) cortex, while the remainder of the brain remained largely unaffected. Subtraction of an image taken from a resting control study from the image obtained in the stimulation study provides a display of the blood flow changes occurring as a result of stimulation.

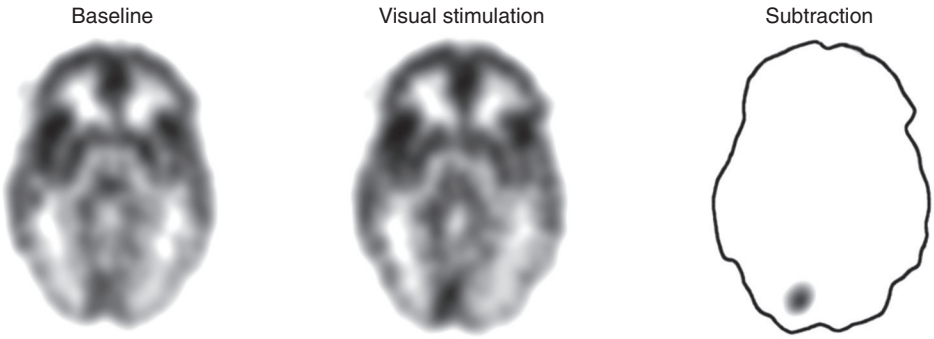

FIGURE 20-8 Cerebral blood-flow images ($H_2{}^{15}O$ PET) acquired in the resting state (*left*) and during visual stimulation using a flashing light (*center*). The stimulus causes a small increase in blood flow in the visual cortex that is virtually invisible on the image acquired during visual stimulation; however, the increase is clearly visible when the resting-state image is subtracted from it (*right*).

Most digital images in nuclear medicine are, in essence, pictures of the count density in the organ or tissue of interest. Instead of presenting the data in this format, one may desire to first process the image data on a pixel-by-pixel basis using a model that represents the functional process and display the calculated result. Such an image, in which the pixel values represent a calculated parameter, sometimes is called a *parametric image*. For example, a digital ventilation image can be divided by a perfusion image to produce a parametric image that shows the ventilation/perfusion ratio. Other examples of calculated functional parameters are discussed in Chapter 21.

2. Regions and Volumes of Interest

Both PET and SPECT can provide semiquantitative, or when all appropriate corrections are applied, quantitative images of the radiotracer distribution in the body. Conventional 2-D images also can provide information about the relative concentration of radiotracer in different areas. *Regions of interest* (ROIs) are used to extract numerical data from these images. The size, shape, and position of ROIs can be defined and positioned by the user, using a selection of predefined geometric shapes (e.g., rectangles, circles). Alternatively, irregular ROIs can be created using a cursor on the image display. The computer then reports ROI statistics such as the mean pixel value, the standard deviation of the pixel values, and the number of pixels in the ROI (Fig. 20-9). Software tools that use edge-detection algorithms also are available for automated definition of ROIs (see Section B.5).

Care must be taken in the use of ROIs to accurately place them on the tissues of interest, especially for applications in which radiotracer uptake or concentration are

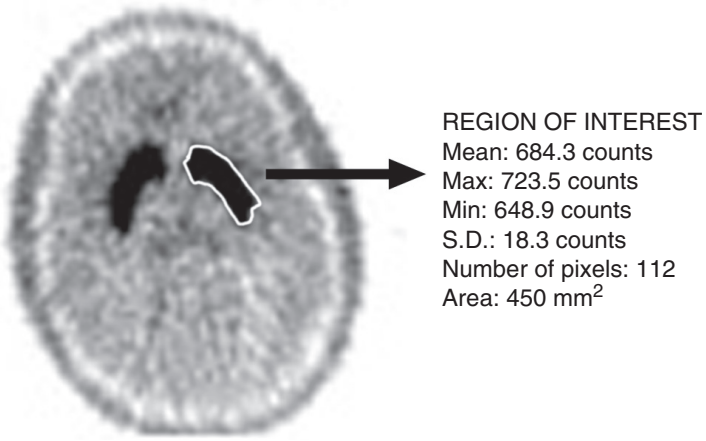

FIGURE 20-9 Manually drawn region of interest (ROI) placed over the right striatum (a small, gray matter structure deep in the brain) in an ^{18}F-fluoroDOPA PET brain study. This tracer reflects dopamine synthesis and accumulates in the dopaminergic (dopamine-producing) neurons of the striatum. Typically, ROI software programs provide a set of statistics on the number of counts per pixel per second (proportional to the radioactivity concentration) and the area of the ROI.

monitored during a longer period. Such measurements sometimes are made, for example, to observe and monitor the metabolic status of a tumor. Automated methods are provided on some computer systems to assist with this task. However, even with an automated method, one must be aware of and careful to avoid errors caused by the partial-volume effects discussed in Chapter 17, Section B.5. For example, an important question for staging in tumor imaging is the concentration of radiotracer in the tumor. A "small" tumor with high uptake (Bq/cm^3) is different from a somewhat larger tumor with low uptake. An apparent increase in radiotracer concentration in a "small" tumor (one that is near the resolution limits of the imaging device) during a longer period actually could be due to tumor growth in size and an associated reduction in partial-volume effects. ROI analysis is therefore particularly difficult when the volume of tissue that is of interest is changing with time.

Most structures of interest extend in all three dimensions and cover multiple image planes in a tomographic dataset. To obtain the best signal-to-noise ratio (SNR), and to ensure that the ROI values are representative of the entire structure, it is necessary to draw ROIs on multiple contiguous image planes that contain the object. In some software these ROIs can be connected to form a *volume of interest* (VOI). Automated tools for defining VOIs also have been developed.

3. Time-Activity Curves

As discussed in Chapter 21, the rate of change of radiotracer uptake in a specific organ or tissue often is of interest. To determine this, the data are acquired as a series of frames over time (see Section A.4). The data typically are analyzed by defining an ROI on one frame, or on the sum of all frames, and then copying the ROI across all of the frames. This is accurate provided that the patient has not moved between frames. The process is illustrated in Figure 20-10 for a time series of images of the brain following the injection of ^{18}F-fluoro DOPA, a compound that localizes in the striatum whose uptake is related to the rate at which dopamine is synthesized.

The ROI data from a series of frames can be used to create a time-activity curve (TAC), showing the radiotracer concentration as a function of time in the tissue defined by the ROI. Figure 20-10 also shows the TAC extracted from the ROI data in the time series of images.

4. Image Smoothing

All nuclear medicine computer systems provide image-smoothing algorithms. Figure 20-11 illustrates the effect of smoothing on an image that has a poor SNR in the unprocessed state. Smoothing operations are, in essence, techniques that average the local pixel values to reduce the effect of pixel-to-pixel variation. Two simple algorithms for 2-D images are 5-point and 9-point smoothing, in which a pixel value is averaged with its nearest 4 or 8 neighbors (Fig. 20-12).

In the previous examples, all four or eight neighboring pixels, as well as the center pixel, are given equal weight in the smoothing process. Image smoothing also can be performed using filters that are weighted according to the distance from the pixel that is being smoothed. One such example is a gaussian smoothing filter. In general, one can write the following:

$$\text{smoothed image} = \text{original image} * \text{smoothing filter} \tag{20-3}$$

where $*$ represents the operation of convolution (see Appendix G). Although smoothing frequently produces a more appealing image by reducing noise (and improving the SNR), it also results in blurring and potential loss of image detail. Sometimes it is convenient to perform analytic studies (e.g., integrating pixel count values over an area) on an unsmoothed image after identifying ROIs on a smoothed image. In such applications, a practical compromise between resolution and visual appeal must be reached.

5. Edge Detection and Segmentation

Edge detection and segmentation are two image-processing tools that can be used to assist in automatically defining ROIs. They also are used for classifying different types of tissue based on their radiotracer uptake and for defining the body and lung contours for attenuation correction (see Chapter 17, Section B.2).

Edge-detection algorithms work best with edges that are very clearly defined as a result of a sharp boundary in radiotracer uptake. One of the most common is the *Laplacian technique.* The 2-D Laplacian is defined by

$$\text{Laplacian} = \frac{\partial^2}{\partial x^2} + \frac{\partial^2}{\partial y^2} \tag{20-4}$$

where $\partial^2/\partial x^2$ represents the second partial derivative of the function [i.e., the pixel

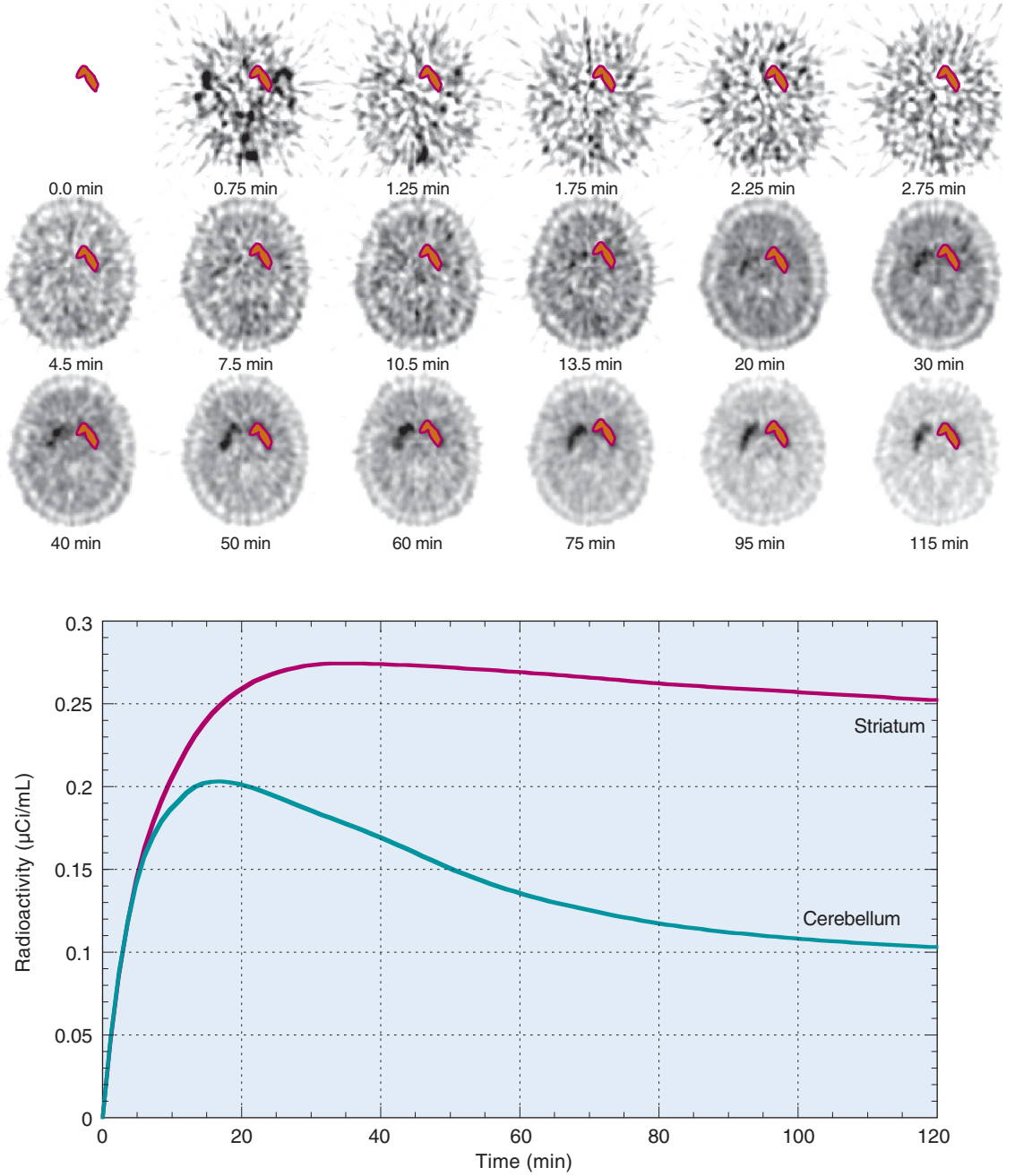

FIGURE 20-10 *Top,* PET images of the same two-dimensional (2-D) slice through the brain at different times after administration of a bolus injection of ^{18}F-fluoroDOPA. A region of interest (ROI) is drawn over the right striatum on the last image and then copied to all other time points. *Bottom,* Time-activity curve (TAC) showing the mean value in the ROI, converted with a calibration factor from counts per second per pixel to absolute concentration of radioactivity, versus time for the striatum. Also shown is a TAC for the cerebellum, taken from a different 2-D image slice, demonstrating how different brain regions can have different kinetics. Analysis of such TACs is discussed in Chapter 21. (*Adapted from Cherry SR, Phelps ME: Positron emission tomography. In Sandler MP, Coleman RE, Patton JA, et al [eds]:* Diagnostic Nuclear Medicine*, 4th ed. Baltimore, Williams & Wilkins, 2002, p. 79.*)

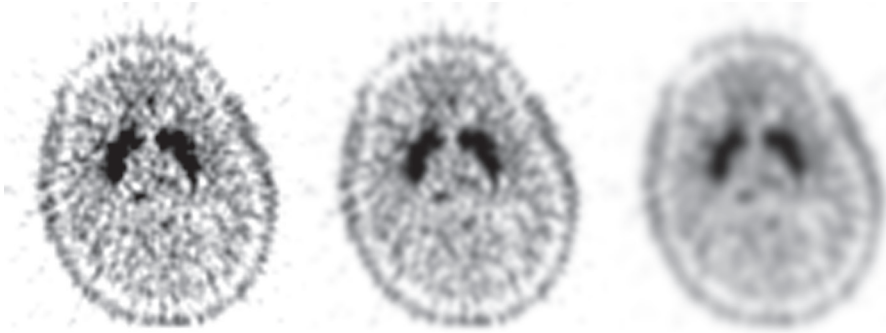

FIGURE 20-11 Effect of image smoothing using a gaussian filter with a full width at half maximum of 4 mm (*center*) and 8 mm (*right*). Smoothing improves the signal-to-noise ratio in the images but at the expense of spatial resolution.

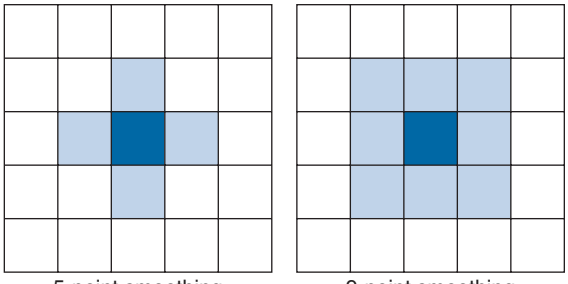

FIGURE 20-12 Illustration of pixels used in 5-point and 9-point smoothing. The value in the pixel of interest (*dark blue*) is averaged with the values in the surrounding pixels (*light blue*).

values, $p(x,y)$], with respect to spatial coordinate x, and similarly for the spatial coordinate y. An analogous definition can be made for the 3-D Laplacian, which would be applied to 3-D datasets. As illustrated by the 1-D example presented in Figure 20-13, the point at which the Laplacian crosses zero represents a region with a high rate of change between neighboring pixel values and therefore reflects an edge. In practice, the operator often specifies a starting point for the algorithm, which then searches in all possible directions and constructs a line (edge) where the Laplacian crosses zero. Eliminating small changes (i.e., setting limits) in the Laplacian reduces the effect of noise. Figure 20-14 shows an image in which the lung contours have been defined automatically by the Laplacian algorithm.

The goal of image segmentation is to group all pixels that have certain defined characteristics. In nuclear medicine, this usually refers to pixels that have a certain range of pixel intensities and thus a certain level of radiotracer uptake. The simplest method of segmentation is just to select pixels having values within a specified range: $A < p(x,y) < B$. Because of image noise, this simple method rarely is sufficient for accurate segmentation. More sophisticated algorithms that consider the underlying resolution and noise properties of the images and that also seek clusters of contiguous pixels usually are employed. Edge-detection algorithms also can be used in segmentation. For example, an edge-detection algorithm can be used to define the contours of the lungs and all pixels within that contour defined as lung tissue. Other examples of edge-detection and segmentation algorithms are discussed in the suggested readings at the end of the chapter.

6. Co-Registration of Images

It is quite common to perform multiple nuclear medicine imaging studies at different times on the same subject. This is useful, for example, to monitor the progression of Alzheimer's or Parkinson's disease, to measure the change in tumor blood flow or metabolism following cancer treatment, or to study the response of brain blood flow to various stimuli. To accurately compare nuclear medicine studies on the same subject performed at different times (e.g., by subtraction of the images), it is necessary that the images be accurately aligned. This is known as *intrasubject intramodality image co-registration.*

Many algorithms have been developed to co-register nuclear medicine studies. They have been particularly successful in the brain, because the brain is rigidly held within the skull and the transformations required to co-register the images are limited to simple translations and rotations. Co-registration accuracy can be as high as 1 to 2 mm. Figure

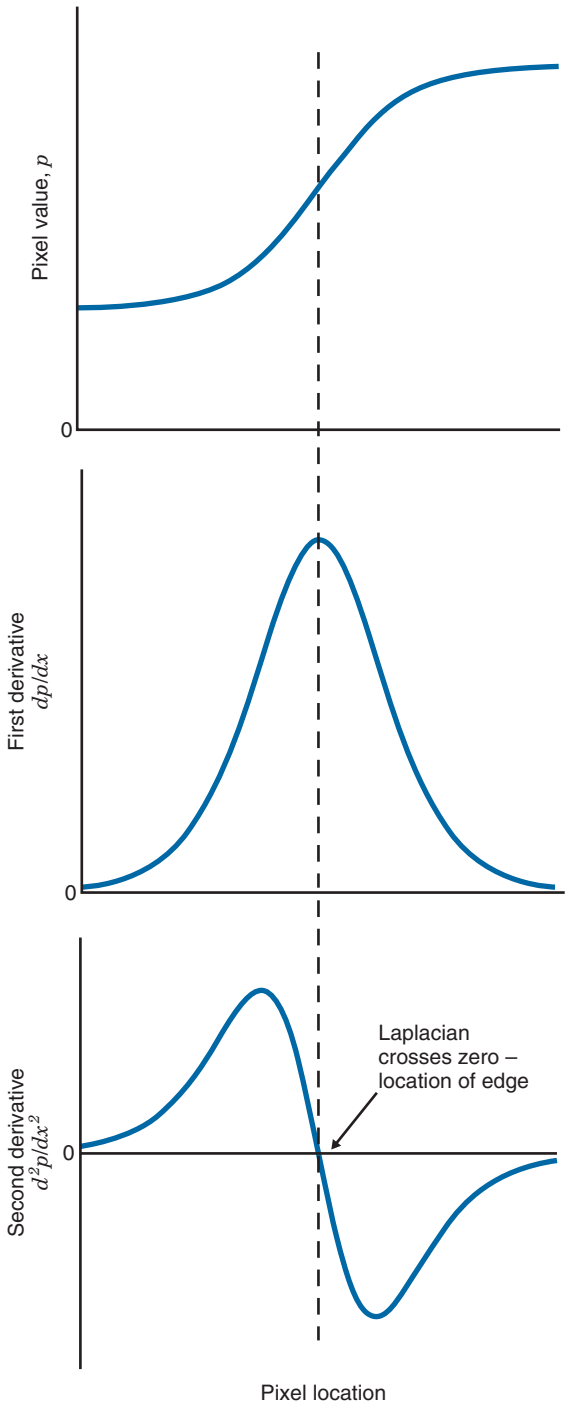

FIGURE 20-13 A one-dimensional example showing a count profile of pixel value p versus pixel location x across a boundary with two different activity levels. The first and second (Laplacian) derivatives of the count profile with respect to x are shown. The first derivative is the difference between neighboring pixel values, or equivalently the local slope of the count profile. At an edge, pixel values are changing rapidly with location and the slope has a high absolute value. The second derivative, the Laplacian, is the difference between adjacent first derivative values. The x-location where this second derivative crosses zero defines the location of the edge.

20-15 shows co-registered PET images of the same subject acquired at different times. Outside the brain, image co-registration becomes much more difficult, because organs can shift relative to each other depending on the exact positioning of the patient on the bed. In general, this requires nonlinear co-registration algorithms that attempt to "warp" one image to fit with the other.

Intrasubject, cross-modality co-registration involves registering a nuclear medicine study with a study of the same subject performed with a different imaging modality (e.g., MRI or CT). This requires more sophisticated algorithms because the information content of the images as well as their spatial resolution and SNR characteristics are different. Nonetheless, algorithms have been successful for co-registering PET and SPECT studies onto MRI or CT images, thereby providing co-registered volumetric datasets that reflect both biologic function (PET or SPECT) and anatomy (CT or MRI). Again, because of its precise geometric relationship to the skull, the most successful applications of these algorithms have been in brain imaging.

There also is interest in intersubject co-registration of nuclear medicine images for comparisons between multiple subjects. For example, this can be used to create images based on a large database of subjects, showing the distribution of a radiotracer across a specific population of subjects. If such a database of images of normal subjects is available for a particular radiotracer, a patient then can be compared with the normal database to see if the distribution is significantly different from normal controls. A summary of modern image co-registration techniques is provided in reference 1.

C. PROCESSING ENVIRONMENT

The digital image-processing environment may be limited to a single gamma camera, or, in a large department, it may involve a collection of gamma cameras and tomographic imaging devices. For all modes of imaging, digital image processing involves several steps: (1) acquisition, (2) processing, (3) display, (4) archiving (storing the raw or processed data or images), and (5) retrieval. Acquisition obviously takes place on the imaging device itself; however, it is useful if the other steps in the chain can be performed not only on the imaging system console but also on any other computers in the hospital or laboratory. In

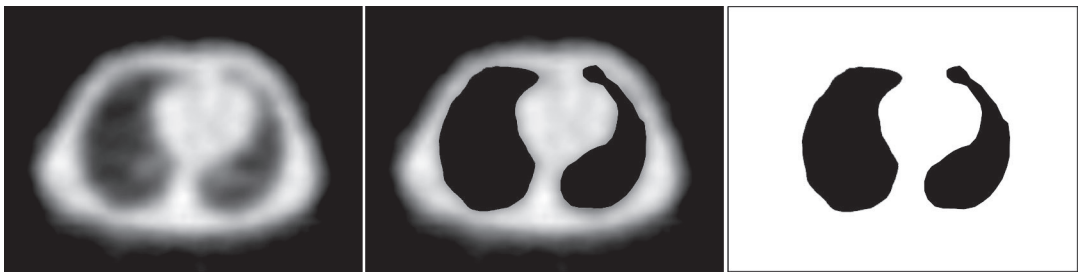

FIGURE 20-14 Series of images illustrating the segmentation of the lungs on a transmission scan acquired on a single-photon emission computed tomography system. (*Original image courtesy Dr. Freek Beekman, University Medical Delft University of Technology, The Netherlands.*)

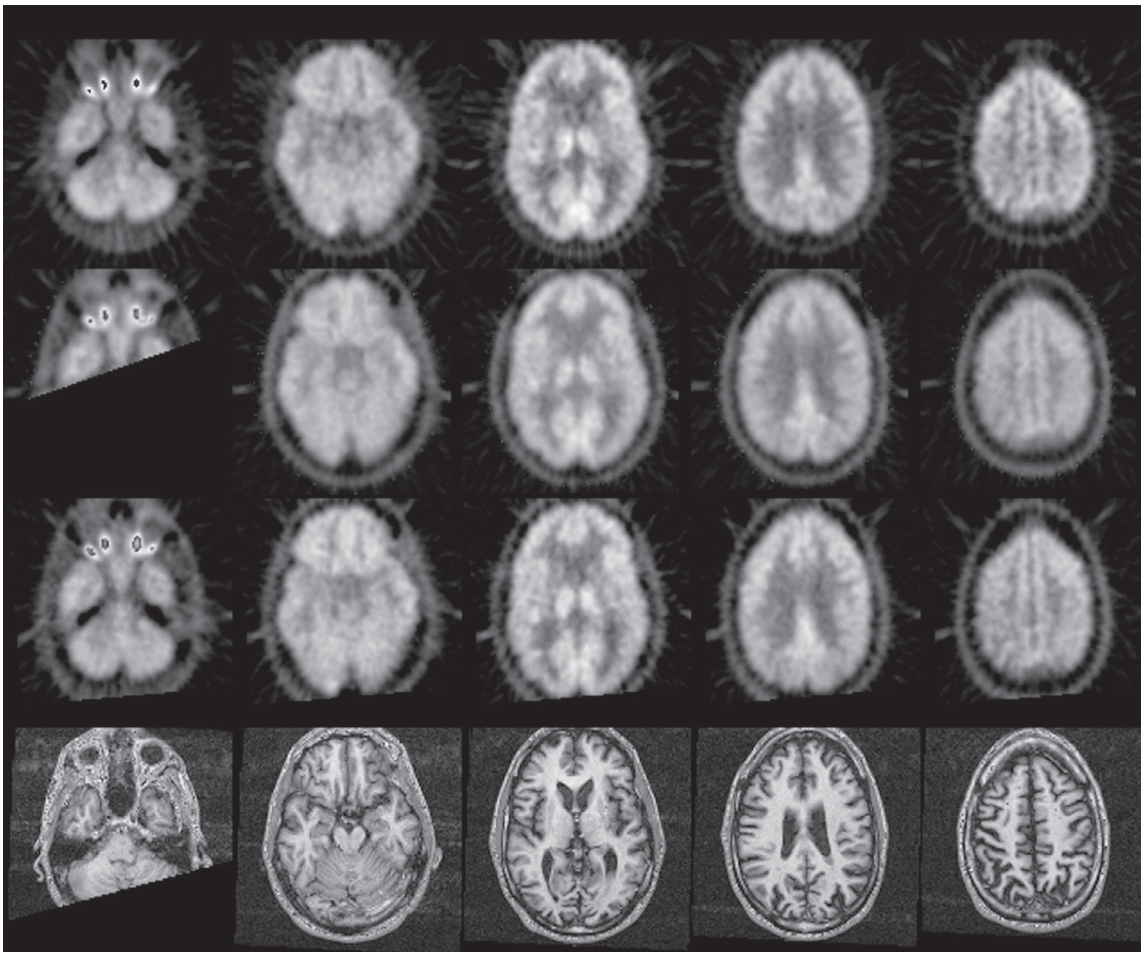

FIGURE 20-15 *Top three rows,* Co-registered slices from three ^{18}fluorodeoxyglucose PET scans acquired at 1-year intervals on the same subject. Images in each column represent the same anatomic slice, after co-registration. *Bottom row,* Corresponding co-registered slices from a magnetic resonance imaging scan acquired at the time of the third PET scan (intermodality co-registration). Images were co-registered using the Automated Image Registration software developed by Roger Woods of the University of California-Los Angeles. Note the excellent agreement in structures included and their locations in each slice. Some images were truncated (particularly in the *left column*) because parts of the brain were outside the field-of-view in some scans. (*From Woods RP, Mazziotta JC, Cherry SR: Optimizing activation methods: Tomographic mapping of functional cerebral activity. In Thatcher RW, Hallett M, Zeffiro T, et al [eds]:* Functional Neuroimaging: Technical Foundations. *San Diego, Academic Press, 1994, p. 54.*)

addition to freeing up the image acquisition computer for additional studies, it allows a variety of other activities to proceed simultaneously. For example, it allows a medical physicist to reprocess a study from his or her office while physicians are viewing the same images in the reading room or even at a different hospital and researchers are downloading the studies onto a computer in the research laboratory.

Many nuclear medicine departments therefore employ high-speed networks to connect their imaging systems together with other computer systems in the institution and, via the Internet, to the outside world. These departments use PACS to store and move images from acquisition sites to more convenient viewing stations and to provide a common basis for handling nuclear medicine and all other diagnostic imaging modalities.[2] PACS systems in hospitals with large radiology and nuclear medicine departments must be capable of handling huge amounts of data, typically several gigabytes per day (1 Gb = 10^{12} bytes).

To facilitate the exchange and handling of images from multiple different imaging modalities and from different vendors each with their own custom software, image file format standards have been developed. The central standard in radiology is the Digital Imaging and Communications in Medicine (DICOM) standard described in reference 3, and all manufacturers producing diagnostic imaging equipment support this standard. The objective of DICOM is to enable vendor-independent communication not only of images but also of associated diagnostic and therapeutic data and reports.

A true archival system not only should store the image or processed image data but also should be organized around a logical retrieval system that permits correlation of images with other types of data (e.g., reports) for a given patient study. That is, it should have the capacity of a computer database system and interface seamlessly with radiology, nuclear medicine, and hospital information systems. In addition, the system must be capable of protecting patient information by providing access only to authorized users.

REFERENCES

1. Hill DLG, Batchelor PG, Holden M, Hawkes DJ: Medical image registration. *Phys Med Biol* 46:R1-R45, 2001.
2. Bick U, Lenzen H: PACS: The silent revolution. *Eur Radiol* 9:1152-1160, 1999.
3. Mildenberger P, Eichelberg M, Martin E: Introduction to the DICOM standard. *Eur Radiol* 12:920-927, 2002.

BIBLIOGRAPHY

General references on image processing

Gonzalez RC, Woods RE: *Digital Image Processing*, ed 3, Upper Saddle River, NJ, 2008, Pearson Prentice Hall. (Chapters 2, 3, 6, and 10 are especially relevant.)
Robb RA: *Biomedical Imaging, Visualization, and Analysis*, ed 2, New York, 1999, Wiley-Liss.